Viscoelastic Behavior of Polymer Tape in a Wound Roll

Katherine Acton, Brian Weick

Department of Mechanical Engineering, University of the Pacific, Stockton, CA

Received 26 May 2010; accepted 22 July 2010
DOI 10.1002/app.34424
Published online 6 July 2011 in Wiley Online Library (wileyonlinelibrary.com).

ABSTRACT: A viscoelastic computational model is developed that uses experimentally determined viscoelastic material properties as input and can be used to predict the behavior of a tape material in a wound roll as stresses relax over time. Experimental creep test results are used to find best-fit creep-compliance parameters to describe two high density data storage tape media. The two tapes used in the analysis are a developmental tape with a poly(ethylenenaphthalate) (PEN) substrate and metal particle (MP) front coat similar to linear tape open (LTO4) (referred to in this work as "Tape C"), and LTO3, a commercially available tape with a PEN substrate and MP front coat. Sets of best-fit creep-compliance parameters are determined for both tapes. The differences between the predicted behavior using three-, five-, and seven-parameter Kelvin–Voigt models are evaluated, both for a benchmark case and in a viscoelastic wound roll model. The choice of material model is found to significantly influence the predictions of the wound roll model. The differences between different material models for the same material are on the order of the differences found between the two different materials. A material model with a higher number of creep-compliance parameters, although more computationally expensive, produces better results, particularly over long spans of time. The relative differences between the three-, five-, and seven-parameter models are shown to be qualitatively consistent for several variations in the computational model setup, allowing predictions to be made based on simple benchmarks. © 2011 Wiley Periodicals, Inc. J Appl Polym Sci 122: 2884–2898, 2011

Key words: viscoelastic properties; relaxation; modeling; mechanical properties

INTRODUCTION

Understanding the long-term behavior of wound magnetic tape is important to the tape industry. As storage capacity increases, and performance characteristics are enhanced, tape continues to be the long-term data storage medium of choice. For many years, thinner tape materials with high volumetric density have been developed to increase the amount of information that can be stored. Currently, increased storage capacity is being achieved by increasing the number of tracks across the width of the tape, which makes mismatch between the read/write element on the head, and the tape tracks a bigger problem.[1] Since these tapes are being marketed as an archival medium for data centers, the tapes must be designed so that the information contained on them is accessible over long periods of time.

Predicting the behavior of the tape material when it is wound into a roll has been the subject of experimental and computational research since tape technology was first introduced. In this work, computational models of the behavior of the wound roll are informed by experimental results which test the constitutive behavior of the individual tape layer over time. Constitutive property parameters are fitted to the results of each experiment. These fitted parameters are used as input into a computational model which simulates the behavior of the wound tape roll over time. The overall result of the experimental and computational work is to develop a predictive model which can be used to aid in the development of tape rolls which undergo minimal deformation over time.

Recent experimental research on the viscoelastic characteristics of current magnetic tape materials has been performed by Weick.[2–4] Specific types of tapes studied include those manufactured to the linear tape open (LTO) format as well as T10000, digital linear tape (DLT), and advanced intelligent tape (AIT) formats. The LTO and T10000 formats typically use poly(ethylenenaphthalate) (PEN) substrates with metal particle (MP) front coats, whereas the DLT uses a PET substrate with an MP front coat. AITs use metal evaporated (ME) front coats applied to an Aramid substrate. General acronyms used for these tape types are MP-PEN, MP-PET, and ME-Aramid. Newer proprietary tapes that use PET substrates with metalized layers applied to each side of the substrate to control dimensional stability have also been used in recent studies.[4] The specific viscoelastic characteristic measured for tapes in the experimental studies is called creep compliance, which

Correspondence to: B. Weick (bweick@pacific.edu).

has typically been measured at elevated temperatures (30, 50, and 70°C). Current studies have also enabled measurements to be performed at low and high relative humidity levels (15% and 75% nominal RH). Results are fitted to a Kelvin–Voigt model to obtain representative compliance and viscosity parameters, which can in turn be used to generate curve fits for the data sets. For the elevated temperature studies, this enables the use of a process called time–temperature superposition to construct extended creep-compliance curves at a reference temperature to predict dimensional stability over extended time periods. The compliance and viscosity parameters are also used as the basis for understanding the behavior of the constitutive tape materials. They can serve as representative property data in computational models that quantify the stress and strain fields in a wound roll.

Computational modeling of stress fields in wound rolls has been performed in the literature for a variety of purposes. A model was developed by Hakiel[5] to investigate the stresses in wound rolls of paper. Though the formulation is only applicable to the linear elastic formulation of the problem, the boundary value problem posed by Hakiel is useful as a benchmark. The one-dimensional Hakiel solution was used as a benchmark solution by Lee and Wickert[6,7] in investigating the stresses developed in an elastic two-dimensional tape layer.

The importance of capturing the viscoelastic nature of polymer tape has long been recognized. Tramposch[8,9] used a four-parameter viscoelastic model to describe the tape layers and obtained results showing the stresses in the wound roll of tape decaying over time. Two different viscoelastic formulations were put forth by Qualls and Good[10] showing a wound roll model for a material described by a three-parameter viscoelastic material model. Other solutions exist for both elastic and viscoelastic tape materials, including Altmann[11] and Willett and Poesch.[12] Heinrich et al.[13] present a finite element based viscoelastic stress relaxation solution. The work of Lin and Westmann[14] provides a solution for the case in which there is viscoelastic winding and pause. It is noted that more solutions exist in the literature for the elastic problem than for the viscoelastic problem, due to the relative complexity of the latter. In this work, the Hakiel[5] model is used as a benchmark, and a viscoelastic model is developed based on the work of Qualls and Good[10] to describe time-dependent behavior in a wound roll.

Results are presented in this work showing the predicted behavior of different viscoelastic materials in a wound roll configuration. The predictive model is sufficiently general to account for the behavior of any tape material, using as input the compliance and viscosity parameters which approximate the material behavior. The materials under consideration here have constitutive parameters which have been determined as a result of experimental analysis; this process is described in the following section.

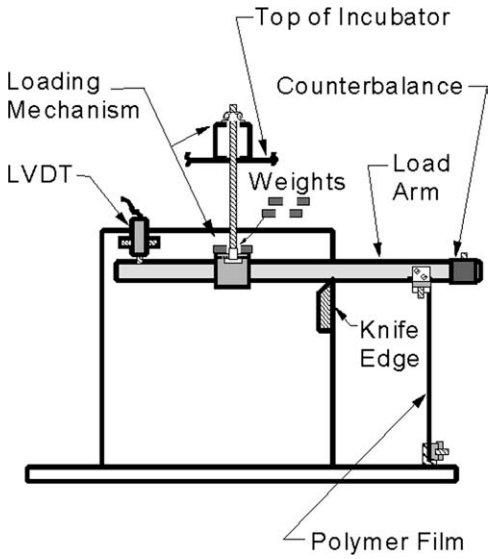

Figure 1 Schematic view of a creep tester for evaluating the creep behavior of magnetic tape materials.[3]

EXPERIMENTAL TESTING OF POLYMER TAPE

As summarized by Weick,[3] experimental creep-compliance data sets used in this study were obtained using a custom-built apparatus housed in a temperature-controlled incubator. A schematic of this test apparatus is shown in Figure 1. Humidity was controlled by using desiccant in the test chamber at low temperatures (30°C); at high temperatures (50 and 70°C) the chamber dries-out, and the humidity was less than 1%. A 330–400 mm long tape samples were evaluated. These samples had 200 mm long test sections and were 12.7 mm wide. Environmental conditions were monitored using a hygrometer and temperature sensor, and the test apparatus utilized linear variable differential transformers (LVDT's) connected to a LabView-based 16-bit A/D system to measure extension or contraction of the samples. The experiments were performed at a 7.0 MPa stress level that corresponds with typical drive tensions.

Using output from the LVDT's, the creep strain, $\varepsilon(t)$, can be determined as well as the creep compliance, $D(t)$, as the initial steps in the viscoelastic analysis.

$$\varepsilon(t) = \frac{\Delta l(t)}{l_0} \tag{1}$$

$$D(t) = \frac{\varepsilon(t)}{\sigma_0} = \frac{\Delta l(t)}{\sigma_0 l_0} \tag{2}$$

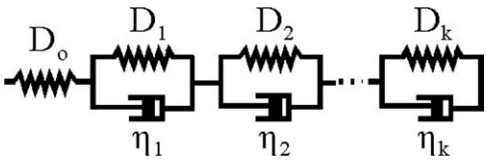

Figure 2 The Kelvin–Voigt model used to express the elastic and viscous characteristics of polymeric materials.[3]

where $\Delta l(t)$ is the change in length of the test specimen as a function of time, l_0 is the original length of the test specimen, $\varepsilon(t)$ is the amount of strain the film is subjected to, σ_0 is the constant applied stress, and $D(t)$ is the tensile creep compliance of the test specimen as a function of time.

Creep-compliance data for the test specimens are modeled using a generalized Kelvin–Voigt viscoelastic model, which has the following mathematical form:

$$D(t) = D_0 + \sum_{k=1}^{K} D_k(1 - e^{-t/t_k}) \quad (3)$$

where D_0 is the instantaneous compliance at time $t = 0$, D_k is the discrete compliance term, and τ_k is the discrete retardation time for each Kelvin–Voigt element. Figure 2 depicts this equation using a mechanical analog consisting of springs with compliances of D_k, and dashpots with viscosities of η_k. Note that each viscosity term is the ratio of the retardation time τ_k to the compliance D_k for each element. In this work, the three specific cases under consideration will be referred to as three-, five-, and seven-parameter models. The three-parameter model is truncated at $K = 1$ in eq. (3) (and includes the three parameters D_0, D_1, and τ_1), the five-parameter model is truncated at $K = 2$ (and includes the five parameters D_0, D_1, D_2, τ_1, and τ_2), and the seven-parameter model is truncated at $K = 3$ (and includes the seven parameters D_0, D_1, D_2, D_3, τ_1, τ_2, and τ_3). As described by Weick[3] as well as Weick and Bhushan,[15,16] five to seven parameters (two to three Kelvin–Voigt elements) are typically required to adequately fit data sets to this model.

Three, five, and seven parameter curve fits to Tape C and LTO3 are shown in Figures 3 and 4, respectively, and the calculated curve fit parameters for each material using each model are shown in Table I. Figure 3 utilizes data sets and curve fits for a developmental PEN-based magnetic tape called Tape C, and Figure 4 utilizes data sets and curves fits for a commercially available LTO3 tape. Both tapes use an MP coating for the magnetic layer. Raw data from the 50°C experiments are shown in gray, and variation in the data is due to the ±0.1°C temperature cycling in the chamber. Top panels in Figures 3 and 4 show the raw data and curve fits on a linear scale; bottom panels show the data and curve fits on log scales. For time periods less than 10 h, the five and seven-parameter curve fits tend to work equally well, but the seven-parameter curve fit works better for longer time periods of 10–100 h.

The creep compliance for Tape C shown in Figure 3 begins decreasing after less than 10 h. As a result, the D_3 and τ_3 terms (listed in Table I) are significantly lower for Tape C when compared with LTO3; they have negative and positive values, respectively. Note that the three- and five-parameter models for Tape C reach peaks at earlier time periods and remain virtually constant after reaching this level. Also, the D_1, τ_1, D_2, and τ_2 parameters for Tape C tend to be lower than that for LTO3. Even the D_0 values for Tape C are smaller than what was measured for LTO3. Weick[3] has reported that the PEN substrate used for Tape C has pronounced shrinkage characteristics when compared with the PEN substrate for LTO3. The negative D_3 values are related

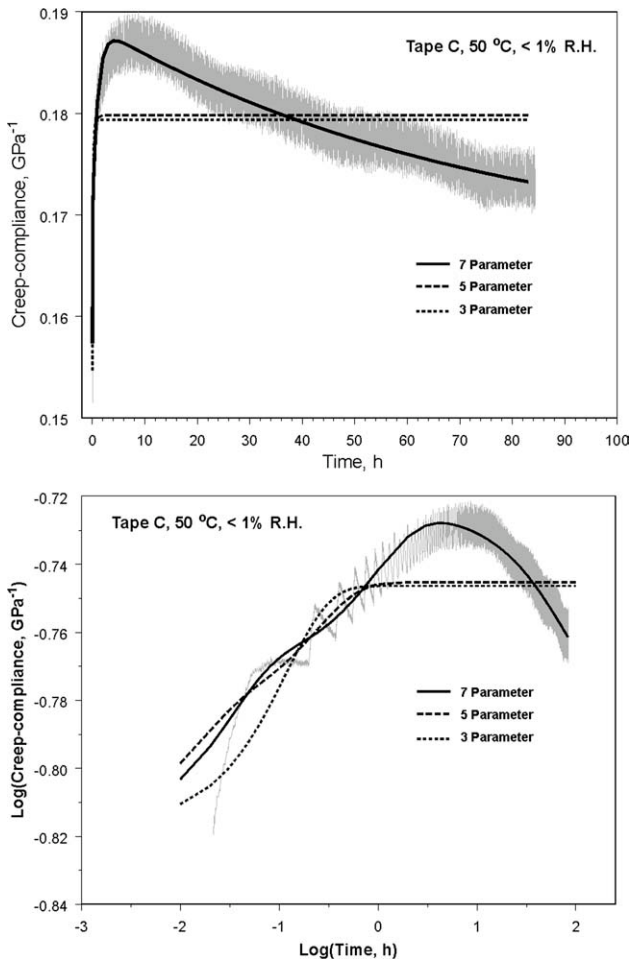

Figure 3 Curve fits using three-, five-, and seven-parameter Kelvin–Voigt model for "Tape C," which is a developmental PEN-based magnetic tape with a metal particle (MP) coating.

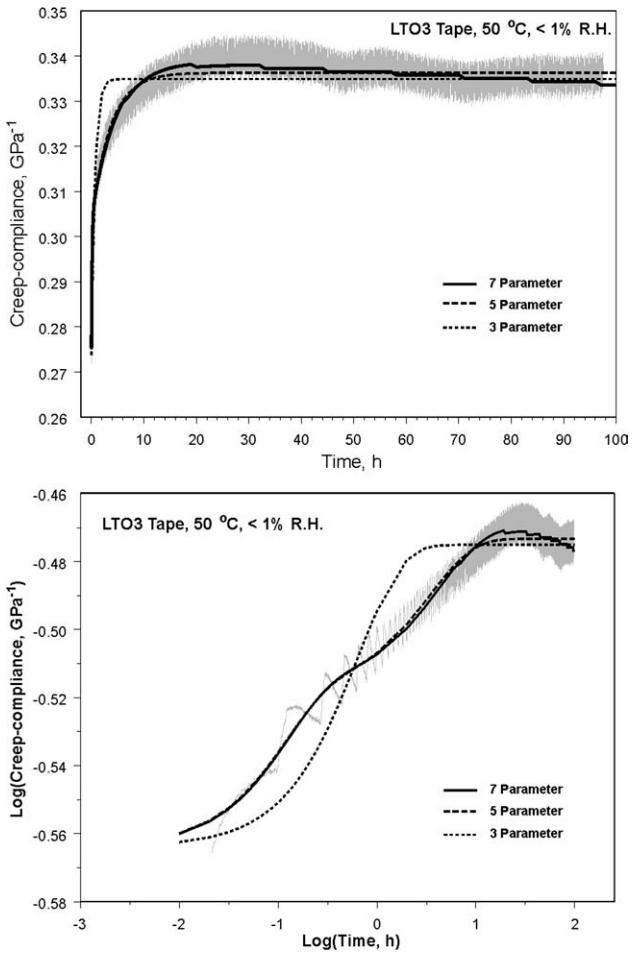

Figure 4 Curve fits using three-, five-, and seven-parameter Kelvin–Voigt models for an LTO3 tape.

to this shrinkage phenomenon, commonly attributed to motion of partially oriented molecules in the amorphous region of the PEN material. This tendency to shrink in addition to creep could contribute to the earlier peak in creep compliance for Tape C followed by a relatively more pronounced decrease over the remaining time period. Other types of relaxation could be occurring in Tape C, which could be attributed to the coating process.[4]

For the LTO3 tape shown in Figure 4, with parameters listed in Table I, there is a similarity between the three- and five-parameter Kelvin–Voigt models when compliance, retardation time, and viscosity parameters are compared. However, the seven-parameter model is a better fit for the data during the 10–100 h time period for the LTO3 tape. Note that the first and second sets of viscoelastic parameters (D_1, τ_1, D_2, and τ_2) are all positive in Table I. In comparison, D_3 is negative for the LTO3 tape, and τ_3 is positive for the third set of parameters. The difference in signs can be attributed to the decrease in creep compliance after $\sim$ 10 h, and the seven-parameter model with the negative D_3 and positive τ_3 terms capture the final part of the data set better than the three- or five-parameter models. Weick[3] points out that the characteristics of the substrate appear to control this behavior. He provides an analysis of these viscoelastic parameters at other temperatures for LTO3 and other MP-PEN tapes.

WOUND ROLL SIMULATION PROCEDURE

Elastic model

The elastic model for predicting stresses in a wound roll stems from the work of Hakiel.[5] The winding problem is treated as a boundary value problem where each wound-on layer is treated as a separate concentric layer, and the resulting stresses caused by the winding on of each layer are superimposed. The coordinate directions used in this work are consistent with the conventional assignments also used in Hakiel, a schematic is given in Figure 5. Each wound-on layer has a tangential stress equal to the tension of winding in the outer layer, and a radial stress related to the tangential stress by the equation for hoop stresses in a cylinder. This condition forms the outer boundary condition. The inner boundary condition is found by setting the displacement at the innermost layer equal to the displacement at the outside of the hub. These two boundary conditions, together with a governing equation based on equilibrium and displacement continuity between the

TABLE I
Experimentally Determined Viscoelastic Creep Parameters for Tape C and LTO3, for Each of the Three, Five and Seven Parameter Models

	Tape C			LTO3		
Parameter	Three	Five	Seven	Three	Five	Seven
D_0 (1/GPa)	0.153	0.153	0.153	0.273	0.273	0.273
D_1 (1/GPa)	0.0267	0.0119	0.0173	0.0619	0.0302	0.0313
τ_1 (h)	0.123	0.0149	0.0327	0.691	0.119	0.127
D_2 (1/GPa)	—	0.0153	0.0189	—	0.0331	0.0352
τ_2 (h)	—	0.246	1.03	—	3.56	4.70
D_3 (1/GPa)	—	—	−0.0230	—	—	−1.23e4
τ_3 (h)	—	—	73.9	—	—	2.15e8

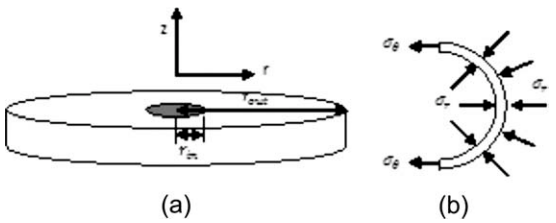

Figure 5 Coordinate definitions in a wound roll. (a) shows the roll and (b) shows the radial and tangential stress in a single layer.

layers, make up a boundary value problem which can be solved numerically for the stress in each layer that is caused by the addition of the current outer layer. The layers are "accreted," until the actual outer layer has been wound on. In this way, tangential and radial stress distributions are found.

One difficulty outlined by Hakiel is the use of the so-called "bulk radial modulus," which describes the radial modulus of the tape roll at a given radial location within the roll. The bulk radial modulus is a function of the interlayer pressure between tape layers, principally because air becomes trapped within each wound-on layer. The bulk radial modulus is therefore generally found to be lower than the modulus of the tape material in the radial direction. Hakiel's formulation allows for the use of a nonlinear bulk radial modulus; it is found that a more precise definition improves the accuracy of the model. The use of a nonlinear bulk radial modulus, which is often empirically based in elastic models, proves to be especially difficult in the viscoelastic case, where the bulk radial modulus is also a function of time. In this work, in both the elastic and viscoelastic models, the bulk radial modulus will be treated as a constant, equal to the isotropic modulus of the tape, which in the viscoelastic case will undergo stress relaxation over time.

Viscoelastic model

As in the elastic Hakiel model, in the one-dimensional viscoelastic model, a boundary value problem is solved for each wound-on layer. The boundary conditions and the method of numerical accretion of layers are similar to the elastic solution, but additionally complex due to the time dependency of the model. The central feature of the viscoelastic model is the use of Laplace transformation to solve the underlying boundary value problem. The time-dependent governing equation used in the analysis is based on a Laplace transform of the time-independent stress distribution calculated by Timoshenko and Goodier[17] for a hollow, axisymmetric, and isotropic cylinder. The approach used in this work is similar to the analytical model developed using a three-parameter material model by Qualls and Good.[10] The goal is to generalize the formulation of Qualls and Good such that any given set of experimentally determined viscoelastic parameters may be used as input into the model.

The governing equation for a hollow axisymmetric cylinder is given in the form developed by Timoshenko and Goodier,[17] where the variables A and C are unknown coefficients, and the radial and tangential locations at which the stresses are to be found are given by r and θ, respectively.

$$\bar{\sigma}_r = \frac{A}{r^2} + 2C \tag{4}$$

$$\bar{\sigma}_\theta = -\frac{A}{r^2} + 2C \tag{5}$$

The overbar on variables in this analysis denotes that the quantities are Laplace transforms of the time-dependent quantities. The problem will be solved in Laplace space, with the results then transformed into the time domain as the final step in the solution to the problem.

To solve for the coefficients A and C, two boundary conditions are required, which must also be expressed as equations in Laplace space. The derivation for these boundary conditions is similar to the formulation given in Qualls and Good,[10] and the formulas for each are given below. The first boundary condition is applied at the hub–tape interface, at $r = r_{in}$:

$$\frac{\bar{\sigma}_r}{\bar{E}_h} = \frac{\bar{\sigma}_\theta}{s\bar{E}} \tag{6}$$

where E_h is the constant elastic stiffness of the hub, $\overline{E}$ is the transformed stiffness of the tape material, and s is the Laplace variable. The second boundary condition is applied at the outer boundary and can be thought of as a viscoelastic formulation of the hoop stress formula in Laplace space. At $r = r_{out}$:

$$\bar{\sigma}_r = -\frac{T_w \bar{E} h}{E_0 r_{\text{out}}} \tag{7}$$

where h is the radial-direction thickness of a single layer, T_w is the tension of winding, and E_0 is the initial stiffness of the tape material. The viscoelastic model presented by Qualls and Good[10] is based on the assumption that the material in each layer can be described by a three-parameter viscoelastic spring–dashpot model, as shown in Figure 2 for the case where only the parameters D_0, D_1, and τ_1 are included. The parameters are assumed to be an input to the model, determined through creep-compliance experiments followed by fitting the data sets to the Kelvin–Voigt model as outlined in the section "Wound Roll Simulation Procedure."

As given by Qualls and Good,[10] the Laplace transform of the strain is the sum of the elastic component ($\bar{\varepsilon}_E$) and the so-called Kelvin component ($\bar{\varepsilon}_K$) connected in series:

$$\bar{\varepsilon} = \bar{\varepsilon}_K + \bar{\varepsilon}_E \tag{8}$$

The transformed stress in each series element is constant, therefore strain can also be expressed:

$$\bar{\varepsilon} = \frac{\bar{\sigma}}{E_1 + \eta_1 s} + \frac{\bar{\sigma}}{E_0} \tag{9}$$

The transformed modulus $\overline{E}$ can be expressed as follows:

$$s\bar{E} = \frac{\bar{\sigma}}{\bar{\varepsilon}} \tag{10}$$

It is noted that the form used in eq. (10) follows the formal definition of the transformed modulus given by Christensen,[18] and slightly differs from the Qualls definition in the treatment of the Laplace variable s. Although this causes no difference between the Qualls solution and the solution obtained in this work, the form given in eq. (10) is a more straightforward form for use in comparing the transformed modulus with the transformed compliance.

Equations (9) and (10) can be combined as follows:

$$s\bar{E} = \left(\frac{1}{E_0} + \frac{1}{E_1 + \eta_1 s}\right)^{-1} \tag{11}$$

The equation for $\overline{E}$ given above is in a relatively simple form, as it relies on only three parameters (E_0, E_1, and η_1) to describe the behavior of the viscoelastic material. More complex forms for the transformed modulus will be developed in the following sections.

Solution of governing equation and accretion of layers in viscoelastic winding

Using the definitions of $\bar{\sigma}_r$ and $\bar{\sigma}_\theta$ given in eqs. (4) and (5), together with the two boundary conditions given in eqs. (6) and (7), the following definitions for the variables A and C are obtained in Laplace space:

$$A = -\frac{T_w h \bar{E} r_{\text{in}}^2 r_{\text{out}} (s\bar{E} - E_h)}{E_0 (s\bar{E} r_{\text{in}}^2 - E_h r_{\text{in}}^2 - s\bar{E} r_{\text{out}}^2 - E_h r_{\text{out}}^2)} \tag{12}$$

$$C = \frac{1}{2}\left(-\frac{T_w h \bar{E}}{E_0 r_{\text{out}}} + \frac{T_w h \bar{E} r_{\text{in}}^2 (s\bar{E} - E_h)}{E_0 r_{\text{out}} (s\bar{E} r_{\text{in}}^2 - E_h r_{\text{in}}^2 - s\bar{E} r_{\text{out}}^2 - E_h r_{\text{out}}^2)}\right) \tag{13}$$

These expressions are used, along with the expression for $\overline{E}$ given in eq. (11), to find the stresses as a function of time by inverse Laplace transform. The functions are defined as follows:

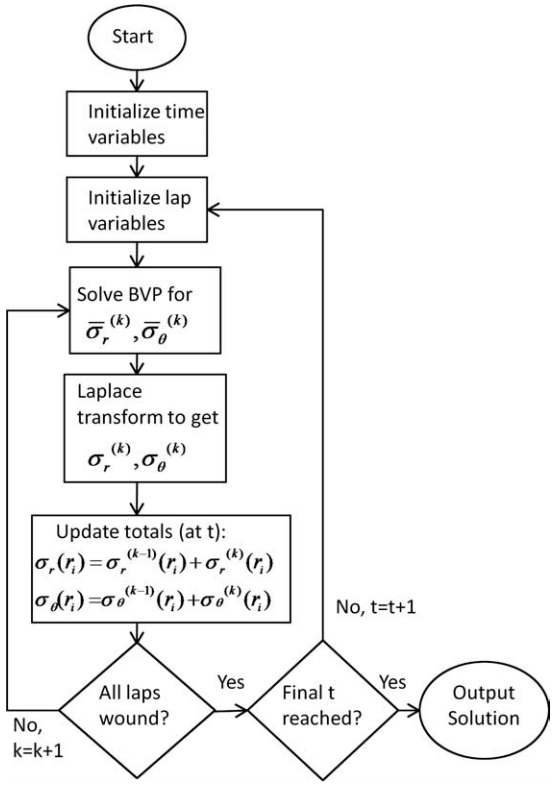

Figure 6 Flow chart depicting the viscoelastic winding algorithm.

$$\sigma_r(r,t) = L^{-1}\left(\frac{A}{r^2} + 2C\right) \tag{14}$$

$$\sigma_\theta(r,t) = L^{-1}\left(-\frac{A}{r^2} + 2C\right) \tag{15}$$

where L^{-1} indicates the inverse Laplace transform operation, and t denotes time. Due to the length of the solution, results for the inverse transform solution are best obtained through commercially available symbolic programming software.

The looping structure of the algorithm used in the full analysis is described as a flow chart in Figure 6. The solution given in eqs. (14) and (15) provides a method for finding the stress developed in the roll as the nth layer is added on. To solve the wound roll problem for the field of stresses as a function of position, it is necessary to use superposition to calculate the combined effects of winding on all layers. The radial stress in a given layer i, where $i = 1, 2, \ldots, N$, where N is the outermost layer, at a given time t_j can be represented by:

$$\sigma_r(r_i, t_j) = \sum_{k=i}^{N} \sigma_r^{(k)}(r_i, t_j) \tag{16}$$

$$\sigma_\theta(r_i, t_j) = \sum_{k=i}^{N} \sigma_\theta^{(k)}(r_i, t_j) \tag{17}$$

The function $\sigma_r^{(k)}$ in eq. (16) denotes the solution of eq. (14) with parameters specific to the kth wound-on layer ($i \leq k \leq N$). A similar equation may be written for the value of tangential stress at a given radius and time and is given by eq. (17). The full wound roll solution is found at a given time; at the next time step the lap variables are re-initialized. The solution is therefore not history dependent; if it is desirable to calculate the stress at a given time, it is not necessary to evaluate prior time steps, nor is it necessary to choose a small time step for convergence. It is however assumed that no unloading or re-loading takes place in the wound roll.

Extension of the viscoelastic model to include additional material property parameters

As detailed in the previous sections, up to seven viscoelastic parameters have been determined for each material in experimental creep testing. One objective in this work is to expand the capability of the underlying Qualls viscoelastic model to incorporate additional viscoelastic model parameters to describe a given polymer tape material.

Before implementation of the experimentally determined creep-compliance parameters into the viscoelastic code, the relationship of the creep parameters (D_i and τ_i) to the stiffness parameters (E_i and η_i) is established. Also, to extend the model to include additional terms, a derivation is performed to establish the Laplace transform stiffness $\bar{E}$ as a function of an increased number of experimentally determined parameters.

The creep-compliance parameters are fitted to the experimentally determined curves based on the following equation for the three-parameter model:

$$D(t) = D_0 + D_1(1 - e^{-t/\tau_1}) \tag{18}$$

First, the correspondence will be shown between eq. (18) and the equation given for the transformed stiffness in eq. (11) for the three-parameter case. The relation between the creep-compliance $D(t)$ and stiffness as a function of time $E(t)$ is given by Christensen[18] as a relation between their transforms in Laplace space:

$$\frac{1}{s^2} = \bar{E}\,\bar{D} \tag{19}$$

Starting with the expression for $D(t)$ given in eq. (18), using the Laplace transform operator to obtain $\bar{D}$, and substituting this value into eq. (19) gives the following:

$$s\bar{\mathrm{E}} = \frac{\mathrm{s}\tau_1 + 1}{D_0 + D_1 + sD_0\tau} \tag{20}$$

Let the relationships between the creep-compliance parameters D_i, τ_i, and the stiffness parameters E_i, η_i be given by:

$$E_i = \frac{1}{D_i} \tag{21}$$

$$\eta_i = \tau_i E_i \tag{22}$$

Substituting the relationships given in eqs. (21) and (22) into the expression for $\bar{E}$ given in eq. (20) yields an expression identical to eq. (11), which is the definition of transformed stiffness used in the Qualls model. Thus, it is shown that the experimentally fitted creep and retardation time parameters may be converted to stiffness and viscosity terms using eqs. (21) and (22), then used as input into the Qualls model.

Next, an extension of the three term model to include additional terms will be presented. Adding an additional term to the creep-compliance $D(t)$ gives the following expression for the five-parameter model:

$$D(t) = D_0 + D_1(1 - e^{-t/\tau_1}) + D_2(1 - e^{-t/\tau_2}) \tag{23}$$

As before, using eq. (19) to relate compliance and stiffness, and performing a Laplace transform on eq. (23) to obtain $\bar{D}$, the following equation is obtained:

$$s\bar{E} = \frac{(1 + s\tau_1)(1 + s\tau_2)}{D_1 + D_2 + sD_2\tau_1 + sD_1\tau_2 + D_0(1 + s\tau_1)(1 + s\tau_2)} \tag{24}$$

If substitutions are made according to the relations given in eqs. (21) and (22), the following is obtained for the resulting value of $\bar{E}$:

$$s\bar{E} = \left(\frac{1}{E_0} + \frac{1}{E_1 + \eta_1 s} + \frac{1}{E_2 + \eta_2 s}\right)^{-1} \tag{25}$$

By a similar analysis, the seven-parameter model has a creep compliance expressed as follows:

$$D(t) = D_0 + D_1(1 - e^{-t/\tau_1}) + D_2(1 - e^{-t/\tau_2}) + D_3(1 - e^{-t/\tau_3}) \tag{26}$$

The Laplace transform stiffness for the seven-parameter model is given as:

$$s\bar{E} = \left(\frac{1}{E_0} + \frac{1}{E_1 + \eta_1 s} + \frac{1}{E_2 + \eta_2 s} + \frac{1}{E_3 + \eta_3 s}\right)^{-1} \tag{27}$$

Using the above equations, the creep-compliance and retardation time parameters obtained as output from the creep experiments may be converted to stiffness and viscosity parameters and used as input

into the Qualls viscoelastic wound roll model. Equations (11), (25), or (27) may be used in the wound roll model, depending on whether the tape material is to be modeled using three, five, or seven parameters, respectively.

Constant strain benchmark solution

Prior to the implementation of the three-, five-, and seven-parameter material models into the viscoelastic winding model, a benchmark solution is tested for each case to illustrate the expected difference between the behavior of the various models. The benchmark solution is for the case where a simple tension T_w is applied to a strip of material, causing the material to undergo a strain of magnitude ε_0 in the direction of the applied tension. The material is then constrained in this direction, and remains unconstrained in any other direction, such that over time the material undergoes stress relaxation in a manner analogous to the relaxation of a wound-on layer of tape. Relaxation is described by each of the three-, five-, and seven-parameter models, and the difference in predicted behavior is examined, as this underlying behavior will inform the analysis of the wound roll results.

The constant strain ε_0 is applied to the strip of material under simple tension, such that $\varepsilon(t) = \varepsilon_0$ at all times t. By properties of Laplace transforms, this implies that in Laplace space:

$$\bar{\varepsilon}(s) = \frac{\varepsilon_0}{s} \tag{28}$$

Using the expression for strain in Laplace space, and the stress–strain relation given for the three-parameter model [eqs. (10) and (11)], the following equation is derived:

$$\bar{\sigma}(s) = \frac{\varepsilon_0}{s}\left(\frac{1}{E_0} + \frac{1}{E_1 + \eta_1 s}\right)^{-1} \tag{29}$$

The inverse Laplace transform function is used to evaluate the stress as a function of time, which gives:

$$\sigma(t) = \varepsilon_0\left(\frac{E_0^2 \exp\left[-\frac{(E_0+E_1)t}{\eta_1}\right]}{E_0 + E_1} + \frac{E_0 E_1}{E_0 + E_1}\right) \tag{30}$$

This function, specific to the three-parameter formulation, can be evaluated in the limit as $t \to 0$, to give the expected elastic solution for a material under simple tension:

$$\lim_{t\to 0} \sigma(t) = E_0 \varepsilon_0 \tag{31}$$

It is also noted that a limit exists for the function as $t \to \infty$, which is given by the following:

$$\lim_{t\to\infty} \sigma(t) = \varepsilon_0\left(\frac{E_0 E_1}{E_0 + E_1}\right) \tag{32}$$

Similar solutions can be derived for the five- and seven-parameter models; these become progressively much more complex due to the inverse Laplace transform operation. Referring to Figure 2, it is expected that for each model of the Kelvin–Voigt form, a nonzero limit state will be reached as time approaches infinity. This is generally true for viscoelastic models that describe solids; for viscoelastic models typically used to describe liquids, with springs and dashpots in series as opposed to in parallel, the limit of stress will approach zero as time approaches infinity. It is noted that spring–dashpot viscoelastic models applied to wound roll stress relaxation are constructed differently in the literature. Most notably, the Tramposh model uses a model which reduces to zero with increasing time. In the current work, the material model chosen dictates that the material in each wound-on layer will retain a finite value of stress even over long time periods, which reaches a plateau value as time increases.

RESULTS AND DISCUSSION

Constant strain benchmark solution

The constant strain benchmark solutions are developed for both materials, using the three-, five-, and seven-parameter models. Results over a short time span ($t = 0$ to $t = 1$ h) are shown in Figure 7, and results over a longer time span, shown on a log scale, are given in Figure 8. These figures can be compared against the experimental results shown in Figures 3 and 4. Figures 3, 7(a), and 8(a) refer to the results for Tape C, and Figures 4, 7(b), and 8(b) refer to the results for LTO3. The same trends which are evident in the experimental results are evident in the constant strain benchmark solutions. For example, in Figure 3, the three- and five-parameter models for Tape C are shown to reach a plateau value, whereas the seven-parameter model fits the data more closely at times greater than 1 h. Figure 8(a) shows the three and five parameters reaching a plateau value of stress relaxation at about 1 h, whereas the seven-parameter model exhibits greater stress relaxation over the time range where its compliance is increasing, up to approximately 80 h. Subsequently, the seven-parameter model exhibits increased stress in the range where its compliance is decreasing.

It is shown using the constant strain benchmark solution that, for the case of Tape C over the first hour of stress relaxation, Figure 7(a), the three-, five-, and

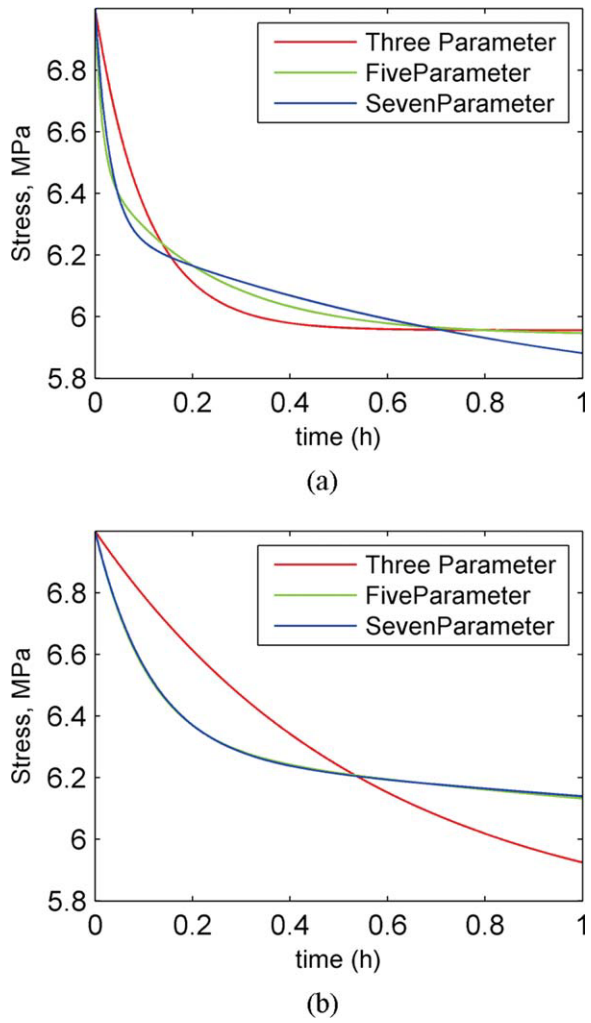

Figure 7 Constant strain benchmark solution showing stress relaxation as a function of time, for (a) Tape C and (b) LTO3. The stress relaxation for each of the three-, five- and seven-parameter models are shown in each case. [Color figure can be viewed in the online issue, which is available at wileyonlinelibrary.com.]

seven-parameter models show notably different trends. At $t = 1$ h, the three- and five-parameter models predict a similar stress value, whereas the seven-parameter model predicts more total stress relaxation over the first hour. For the case of LTO3, shown in Figure 7(b), the five- and seven-parameter models predict essentially the same behavior over the first hour of stress relaxation. These results can be compared against the experimental results shown in Figure 4. The three-parameter model, in both the experimental and the constant strain benchmark case, is initially an outlier, predicting significantly more stress relaxation. Over a long time span, shown in Figure 8(b), the three- and five-parameter models predict that the LTO3 material reaches a similar stress plateau, whereas the seven-parameter model continues to exhibit nonlinear, nonconstant behavior. This result can be compared with the experimental curve fitting shown in Figure (4), which depicts the same trends.

Figure 9 shows the behavior of the two tapes compared against each other, using a five-parameter model in each case, and showing a time range of $t = 0$ to $t = 1$ h. The behavior of the two tapes shows a similar trend, with the LTO3 tape exhibiting less stress relaxation behavior at every time during this interval. Having established the benchmark behavior of the tape materials predicted using the different material models, the behavior of the tape material in the wound roll configuration is now considered.

Relative accuracy of the three-, five-, and seven- parameter material models

In Figure 10, the viscoelastic wound roll model is compared against the elastic wound roll solution to establish accuracy at time $t = 0$. Since the elastic and

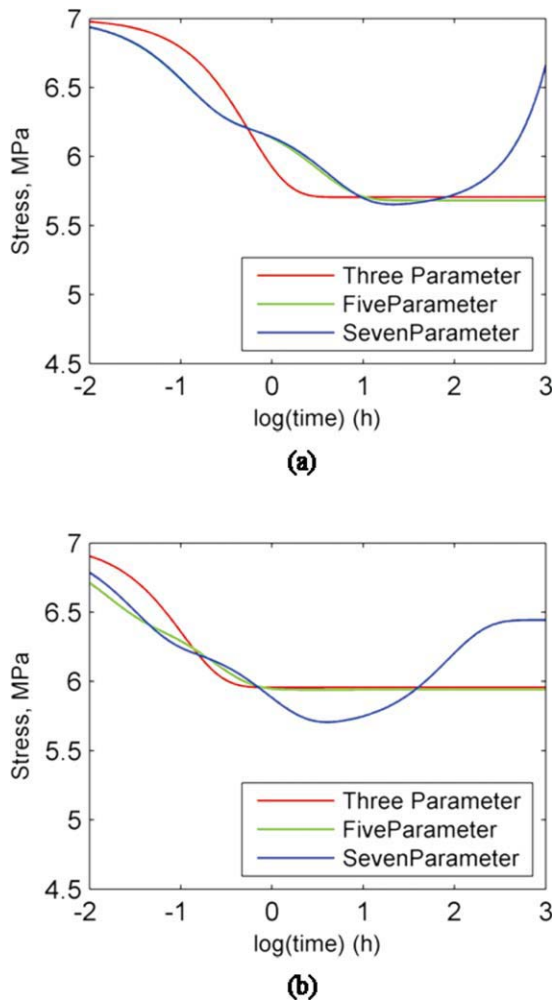

Figure 8 Constant strain benchmark solution showing stress relaxation as a function of time on a log scale, for (a) Tape C and (b) LTO3. The stress relaxation for each of the three-, five-, and seven-parameter models are shown in each case. [Color figure can be viewed in the online issue, which is available at wileyonlinelibrary.com.]

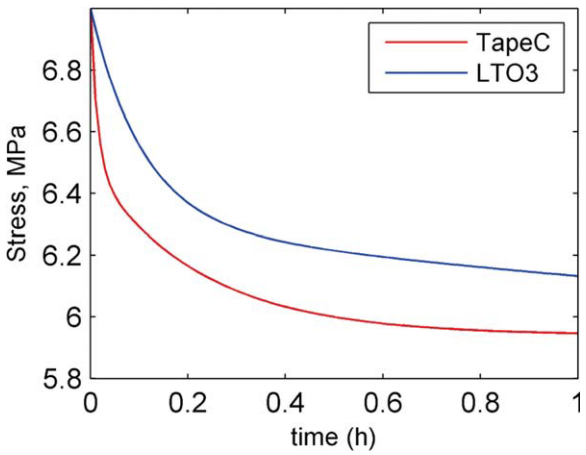

Figure 9 Constant strain benchmark solution comparing the five-parameter LTO3 and Tape C stress relaxation over time. [Color figure can be viewed in the online issue, which is available at wileyonlinelibrary.com.]

viscoelastic models use different governing equations, it is important to reconcile the behavior of the two models. The viscoelastic solution using any number of material property parameters should reduce to the elastic solution at time $t = 0$. In Figure 10(a), the radial stress is shown as a function of radial position in the roll, and in Figure 10(b), the tangential stress is shown. In both cases, good agreement is seen between the elastic and viscoelastic models, and nearly exact agreement is seen between the three viscoelastic models. The agreement between the viscoelastic models shows that numerical rounding error due to the extensive Laplace transform calculations, particularly in models with a higher number of parameters, does not appear to significantly affect the results.

Viscoelastic wound roll results for three-, five-, and seven-parameter models

The viscoelastic wound roll results shown in Figures 11–14 show trends which are also seen in the constant strain benchmark solution. Differences are seen between the behavior of the two tapes, and between the behavior of the same tape predicted using different models. In comparing the differences between the models, simplifications are made to highlight the model differences. In each of the cases considered in Figures 11–14, the hub is assumed to be approximately rigid, and the effect of Poisson's ratio is neglected. The radial modulus of the bulk roll is assumed to be a constant value, equal to the radial stiffness of the tape. The tension of winding in every case is taken to be constant at 7 MPa. It is noted that the wound roll model is similar to the constant strain benchmark in that an initial stress is applied, and an initial strain is developed in each layer as it is wound on. After this point, the strain in each layer is held constant while the stress relaxes. This is similar to the physical behavior of a wound roll, although it is clearly a simplification, because in the wound roll each layer is affected by the accretion of layers subsequently wound on. The constant initial value of applied winding tension ensures that the initial stress profiles of LTO3 and Tape C will be identical under the above assumptions, because the stresses are prescribed. The differences in the wound roll stress profiles of the two tapes become apparent after the onset of relaxation.

In Figure 11, the radial stress as a function of nondimensional radial position for Tape C is shown for times ranging from $t = 0$ to $t = 1$ h. Figure 11(a–c) shows the results predicted by the three-, five-, and seven-parameter models, respectively. These results

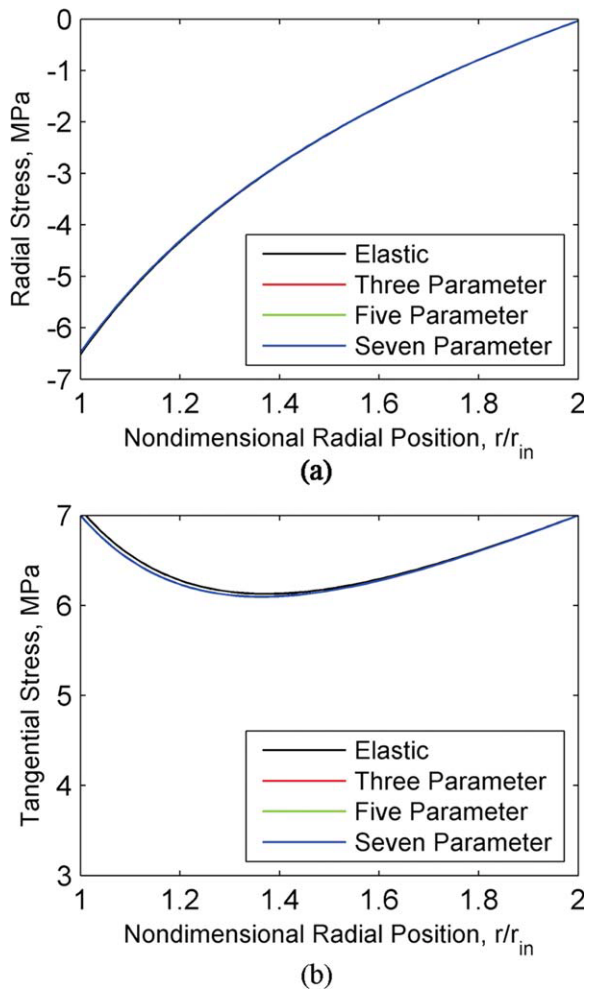

Figure 10 Wound roll stress as a function of nondimensional radial position in a wound roll of LTO3. Radial stress is shown in (a) and tangential stress is shown in (b). The elastic (Hakiel) case is compared with the results for each of the three-, five-, and seven-parameter models where time is set to zero and the viscoelastic case reduces to an elastic analysis. [Color figure can be viewed in the online issue, which is available at wileyonlinelibrary.com.]

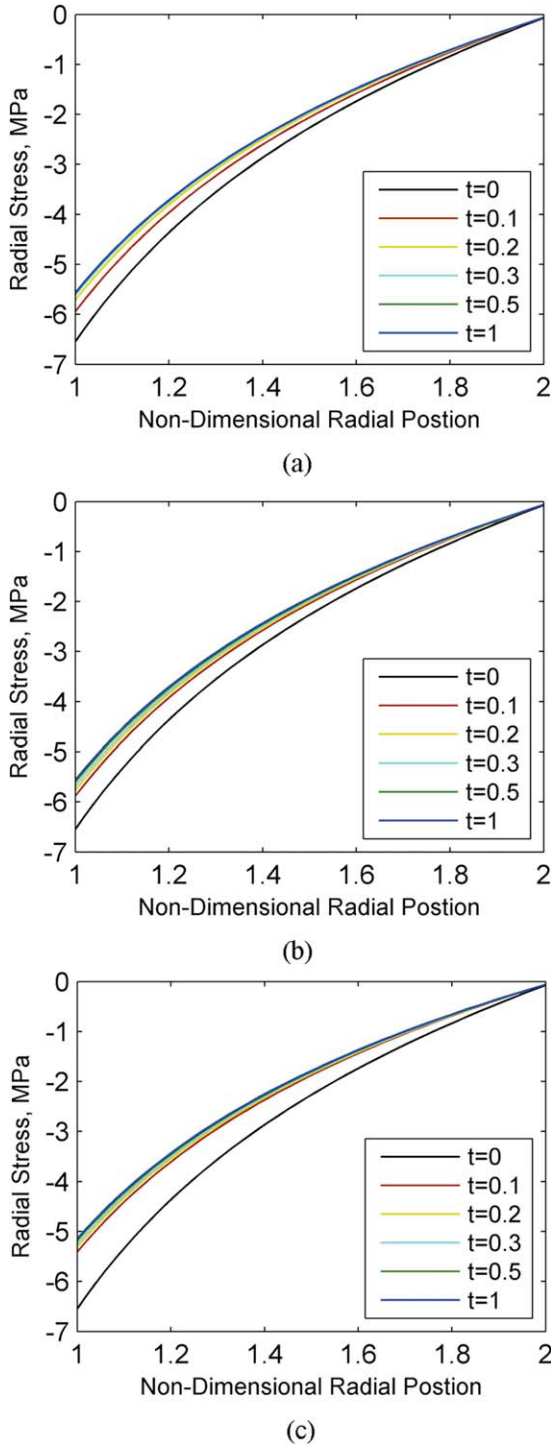

Figure 11 Radial stress as a function of nondimensional radial position in the wound roll for Tape C at times ranging from 0 to 1 h. (a) shows the results using the three-parameter model, (b) shows results using the five-parameter model, and (c) shows results using the seven-parameter model. [Color figure can be viewed in the online issue, which is available at wileyonlinelibrary.com.]

may be compared against the constant strain benchmark solution given in Figure 7(a). As shown in the constant strain benchmark solution, the three- and five-parameter models reach essentially the same relaxed stress value at $t = 1$ h. The five-parameter model shows a sharp initial decrease in stress, followed by a more gradual relaxation, when

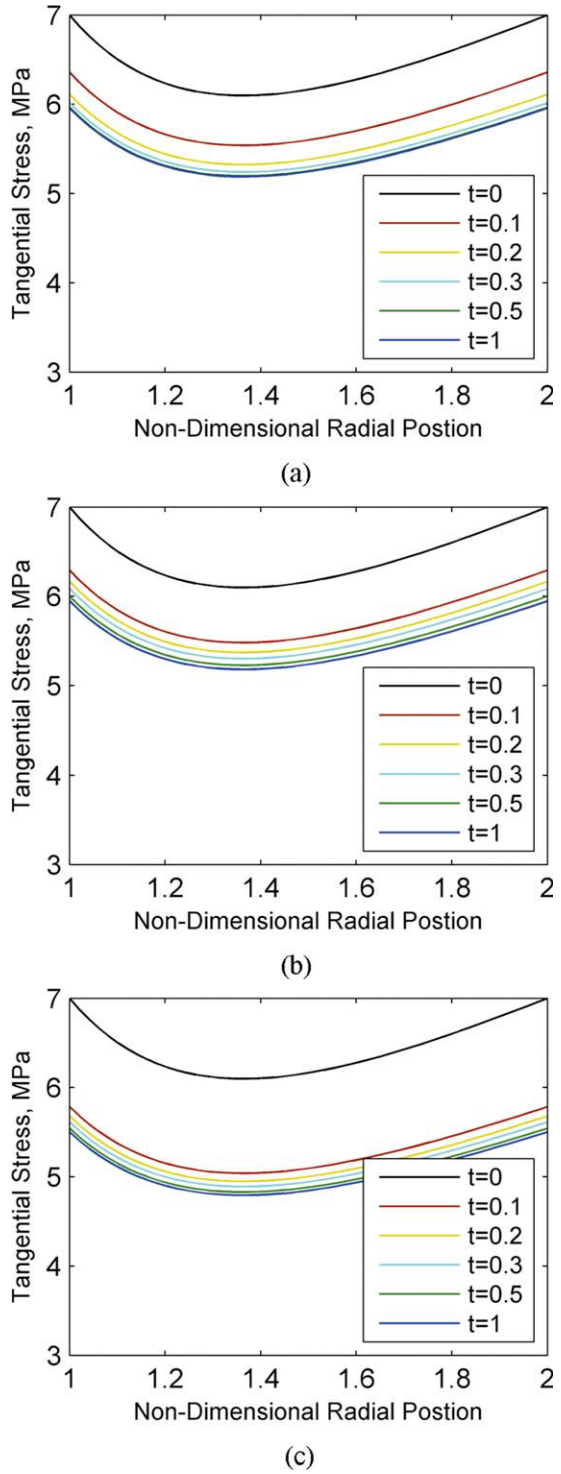

Figure 12 Tangential stress as a function of nondimensional radial position in the wound roll for Tape C at times ranging from 0 to 1 h. (a) shows the results using the three-parameter model, (b) shows results using the five-parameter model, and (c) shows results using the seven-parameter model. [Color figure can be viewed in the online issue, which is available at wileyonlinelibrary.com.]

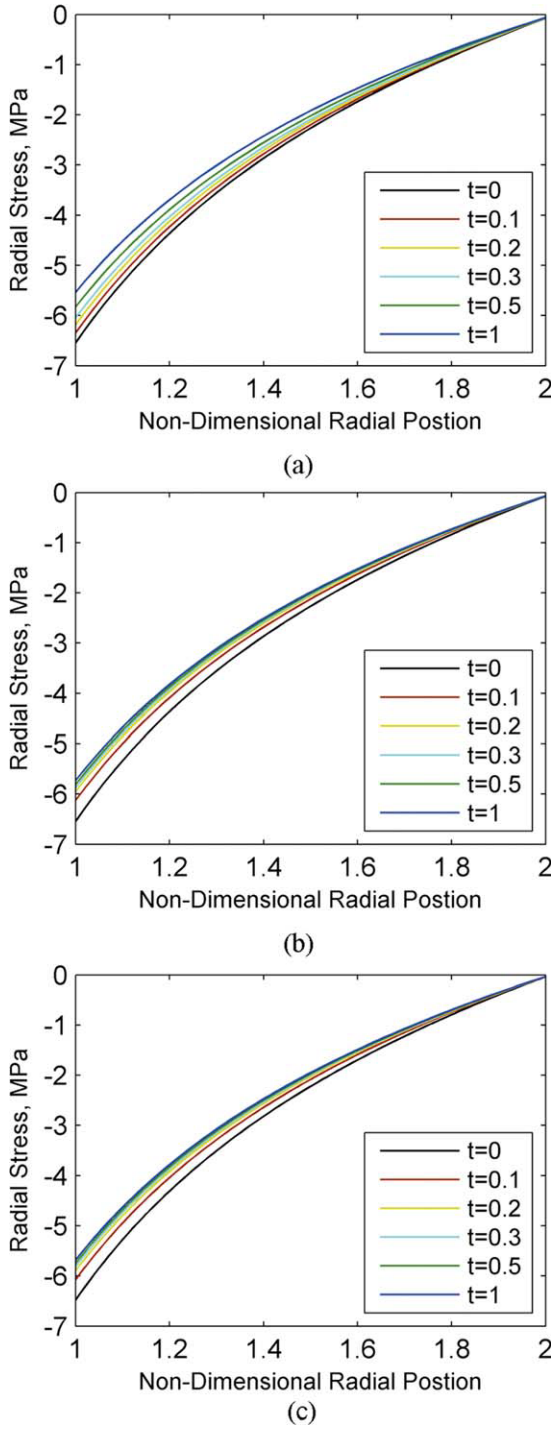

Figure 13 Radial stress as a function of nondimensional radial position in the wound roll for LTO3 at times ranging from 0 to 1 h. (a) shows the results using the three-parameter model, (b) shows results using the five-parameter model, and (c) shows results using the seven-parameter model. [Color figure can be viewed in the online issue, which is available at wileyonlinelibrary.com.]

compared with the three-parameter model. The same trends are evident in the wound roll results shown in Figures 11(a) and 8(b). After 1 h, the results appear the same, though the five-parameter wound roll model shown in Figure 11(b) exhibits a greater stress relaxation between $t = 0$ and $t = 0.1$ h than does the three-parameter model. The seven-parameter model, shown in Figure 11(c) shows more stress relaxation over the first hour in the material in the wound roll, as does the benchmark seven-parameter constant strain solution, shown in Figure 7(a). The results for the tangential stress as a function of nondimensional radial position for Tape C over the same time range are shown in Figure 12. Figure 12(a–c) shows the results predicted by the three-, five-, and seven-parameter models, respectively. The results for tangential stress are identical in trend to the radial stress results and are also supported by the benchmark solutions shown in Figures 7(a) and 8(a).

Similarly, the radial and tangential stress results for the LTO3 tape, shown in Figures 13 and 14, respectively, can be usefully compared against the constant strain benchmark for LTO3, shown in Figures 7(b) and 8(b). For the case of LTO3, it has been shown using the constant strain benchmark solution that the five- and seven-parameter models give very similar results in quantifying stress relaxation in the material for times up to 1 h, whereas the three-parameter model predicts a larger amount of relaxation of stress at $t = 1$ h. This trend is again seen in the wound roll results. Figure 13(a–c) shows the radial stress results predicted by the three-, five-, and seven-parameter models, respectively. Figure 13(b,c) shows very similar results, whereas Figure 13(a) shows a greater relaxation of stress predicted by the three-parameter model. The same result is shown for the tangential stress as a function of radial position, shown in Figure 14(a–c) for the three-, five-, and seven-parameter models, respectively. The three-parameter model shown in Figure 14(a) predicts more relaxation of stress in the wound roll. The relatively shallow slope of the three-parameter constant strain results shown in Figure 7(b) is reflected in both Figures 13(a) and 14(a), which show gradual decline in stress over time.

As in the case of the constant strain solution comparison given in Figure 9, it is also possible to compare the predicted wound roll results for the two tapes against each other. For the case of the five-parameter model, at time $t = 1$ h, a comparison between the behaviors of the two materials is given in Figure 15. The LTO3 is shown to exhibit less stress relaxation within the wound roll than does the Tape C material. This result agrees with the benchmark constant strain solution (Fig. 9). It is noted that the differences between the behavior of the two materials under constant strain loading, or in the wound roll model, are slight. The differences between the two materials may be of approximately the same magnitude, or even less than, the

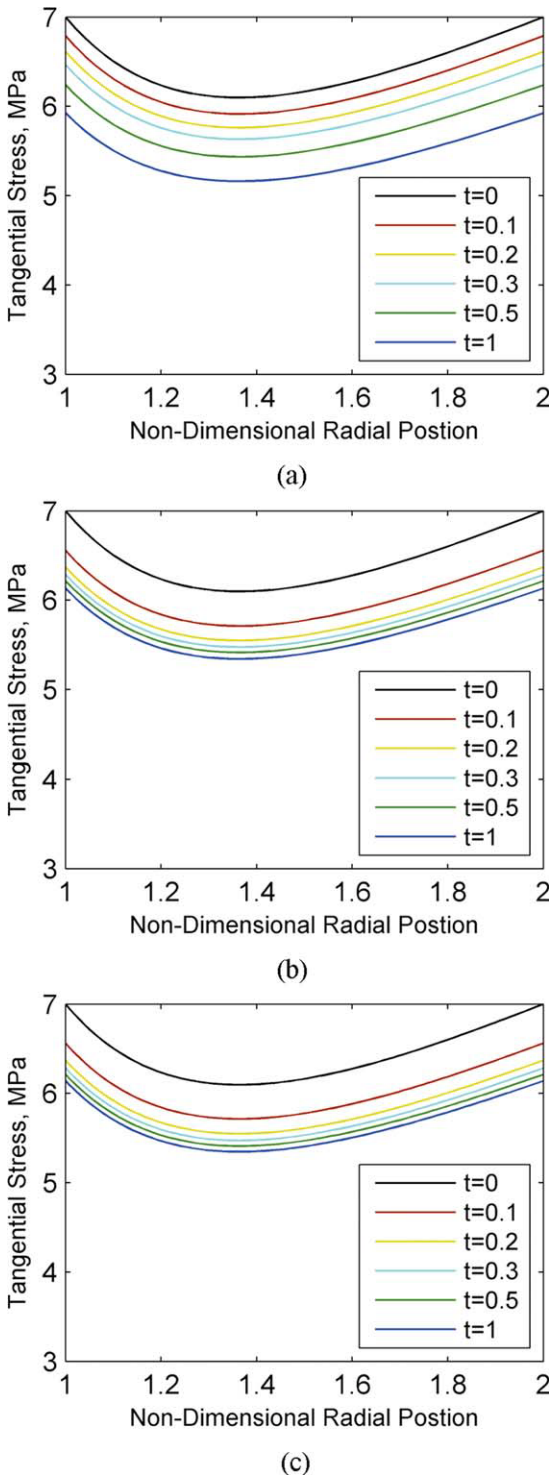

Figure 14 Tangential stress as a function of nondimensional radial position in the wound roll for LTO3 at times ranging from 0 to 1 h. (a) shows the results using the three-parameter model, (b) shows results using the five-parameter model, and (c) shows results using the seven-parameter model. [Color figure can be viewed in the online issue, which is available at wileyonlinelibrary.com.]

differences between the behavior of the same material predicted using different sets of viscoelastic parameters. This result is shown in comparing Figure 15 with Figure 16, which shows two different material models (the three- and five-parameter models) of the same tape (LTO3). The difference between the results predicted by different models (Fig. 16) is similar to the difference predicted between different tapes (Fig. 15). This result underscores the need to accurately capture the material behavior in the viscoelastic parameters used in the model and to choose an appropriate number of viscoelastic parameters. Material property behavior must be captured as accurately as possible before the subtle differences between two types of tapes may be evaluated with accuracy.

To this end, especially over long time periods, it may be advantageous to use a model with a higher number of descriptive parameters. In this case, the seven-parameter model is shown to more accurately capture the behavior of the material at long times (see Figs. 3 and 4). A model with a larger number of parameters is capable of capturing the characteristic roll-off behavior observed for PEN-based tapes and substrates, which could be attributed to relaxation characteristics of the polymer and/or shrinkage.[3,4] Figure 17, showing the radial stress in the wound roll as a function of nondimensional radial position for a seven-parameter model of LTO3, illustrates the effect of the increased stress described by the seven-parameter model at long time ranges. The stress fields in the wound roll are also predicted to increase in stress at long times.

As noted, simplifications and assumptions have been made in predicting the stresses in the wound roll. A more complex model, for example, a model which predicts a nonlinear, variable modulus for the wound roll in the radial direction, would improve the accuracy of the stress field predictions. However, it is expected that the trends in behavior predicted

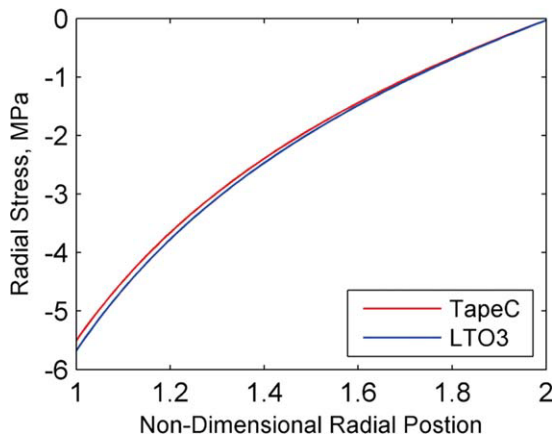

Figure 15 Radial stress as a function of nondimensional radial position in the wound roll for Tape C and LTO3. Both materials are modeled using the five-parameter model at time $t = 1$ h. [Color figure can be viewed in the online issue, which is available at wileyonlinelibrary.com.]

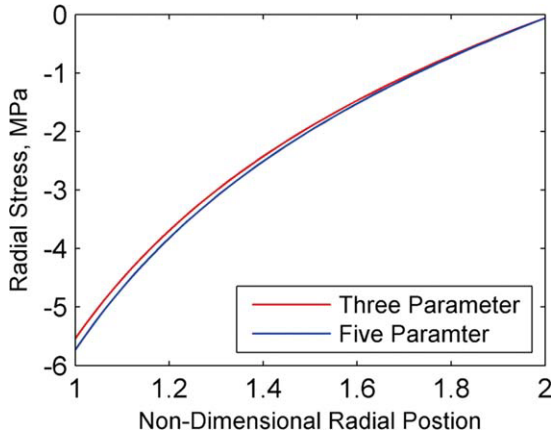

Figure 16 Radial stress as a function of nondimensional radial position for LTO3 evaluated using the three- and five-parameter models. Both models are evaluated at t = 1 h. [Color figure can be viewed in the online issue, which is available at wileyonlinelibrary.com.]

by models using different underlying sets of viscoelastic parameters will persist as the viscoelastic model becomes more complex. For any viscoelastic wound roll model which assumes that tangential stress in each wound-on layer is initially equal to the tension of winding, and the strain in each layer remains constant over time, the constant strain benchmark analysis is expected to inform the wound roll results.

Effect of hub stiffness on wound roll stresses

In the cases shown in Figures 10–17, a high elastic modulus of 10^{20} MPa is used to approximate a rigid hub. In Figure 17, the tangential stress results are shown for an LTO3 wound roll for the case where the elastic modulus of the hub is given as 10^3 MPa,

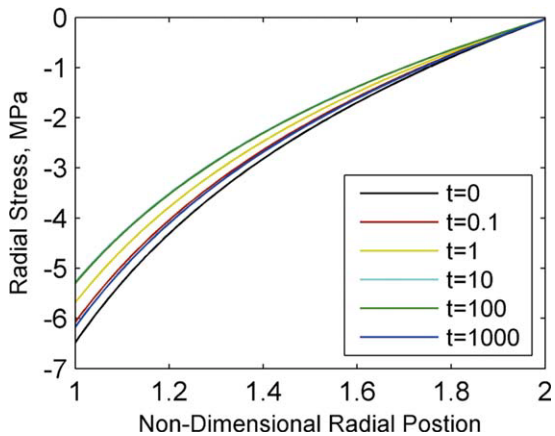

Figure 17 Radial stress as a function of nondimensional radial position in the wound roll for LTO3 at times ranging from 0 to 1000 h. The viscoelastic model used has seven parameters and exhibits shrinkage behavior at long time spans. [Color figure can be viewed in the online issue, which is available at wileyonlinelibrary.com.]

which is closer to the initial stiffness of LTO3 (3.66 MPa). These results are given for the three-parameter model [Fig. 18(a)] and the five-parameter model [Fig. 18(b)]. Figure 18(a,b) can be directly compared against Figure 14(a,b) which shows the same stress relaxation curves for a wound roll with an approximately rigid hub. The trends shown are the same; the three-parameter model shows greater overall stress relaxation at time t = 1 h, with a more gradual decrease in stress over time. This observation is true regardless of the hub stiffness used in the analysis.

In both cases, it is observed that a lower hub stiffness causes stresses to decrease in the tape roll, particularly near the hub. The shape of the curves describing tangential stress as a function of time changes as the hub stiffness changes. However, the comparative differences between the three- and the five-parameter models [Figs. 14(a,b) and 18] are shown to remain essentially the same. As the

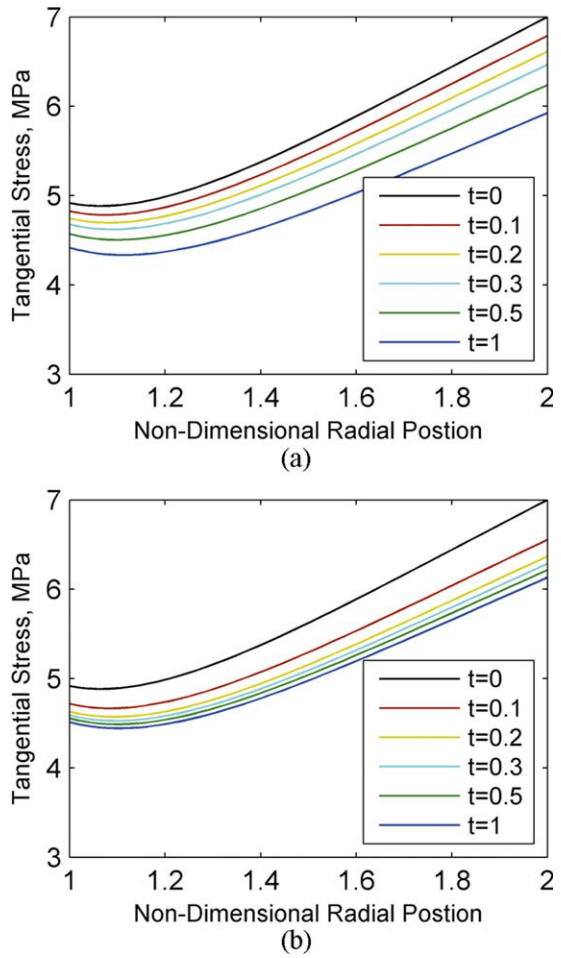

Figure 18 Tangential stress as a function of nondimensional radial position for (a) a three-parameter model and (b) a five-parameter model. In both cases, the stiffness of the hub is set to the relatively low value of 10 GPa, and the material under consideration is LTO3. [Color figure can be viewed in the online issue, which is available at wileyonlinelibrary.com.]

geometry of the model is changed, or as complexity is added to the model, the comparative differences between material models are shown to be unchanged, and are expected to remain valid. For example, it is expected that the further development of the viscoelastic model to include a nonlinear bulk radial modulus would also cause a significant change in the shape of the curves that describe tangential and radial stress as a function of radial position. This result is shown by Lee and Wickert,[6,7] where an investigation is also performed into the effect of hub and flange geometry on the stresses in an elastic wound roll. Although further study is needed on varying hub and flange geometry for a two-dimensional roll composed of viscoelastic tape material, the comparative differences between the three-, five-, and seven-parameter models are expected to remain consistent with respect to such changes in roll geometry.

CONCLUSIONS

A method has been developed for using experimentally determined creep-compliance data as the basis for a viscoelastic computational model of stresses in a wound roll. A constant strain benchmark solution is also developed, which reflects the behavior in a single layer of tape held under a constant strain developed due to the initial application of winding tension. This simple model can be used to obtain qualitative predictions of wound roll results using different material property definitions. For example, if the five- and seven-parameter models give nearly identical results in the constant strain solution, as they do in the case of LTO3 for the time span of 0–1 h, then the same similarity will also be present in the wound roll results. In this case, the five-parameter model would be simpler to evaluate and would produce nearly identical results. However, as time increases, the seven-parameter model captures the distinctive increase in stress in the LTO3 tape material, and would be the more appropriate model for use over long time spans.

The constant strain benchmark solution may also be used to evaluate the expected differences between two or more tape materials over time ranges of interest. In the case of LTO3 and Tape C, as noted, the differences between the predicted behaviors of the two tapes are at times on the order of magnitude of the differences between models of the same material using different parameter models. This result highlights the need for accuracy in material property modeling when comparing the behavior of different tape media in a wound roll.

Results show that a change in hub stiffness affects both the magnitude and the shape of the stress distribution as a function of radial position, particularly at points near the hub boundary. However, the comparisons between results obtained using different material models remain qualitatively unchanged. The results obtained from the constant strain benchmark case (for example, the higher predicted stress relaxation over 1 h in a three-parameter model of LTO3 than in a five-parameter LTO3 model) apply also to the wound roll model, independent of the choice of hub stiffness.

Future work will focus on increasing the complexity of the numerical model, in conjunction with further experimentation to obtain additional viscoelastic input parameters to the model. The model may be usefully generalized to an orthotropic model and to account for the behavior of a nonlinear bulk roll modulus. The results obtained in this work show the consistency of the qualitative comparison between different material property models. Relationships between the results obtained using different material property models are consistent for the study of creep compliance, relaxation under constant strain, and relaxation in a wound roll. It is expected that as the predictive model increases in complexity, the three-, five-, and seven-parameter models will retain the comparative relationships outlined in this work.

The authors would like to acknowledge the members of the INSIC tape program for their support.

References

1. International Magnetic Tape Storage Roadmap; Information Storage Industry Consortium: San Jose, CA, January 2008.
2. Weick, B. L. J Appl Polym Sci 2006, 102, 1106.
3. Weick, B. L. J Appl Polym Sci 2009, 111, 899.
4. Weick, B. L. J Appl Polym Sci 2011, 120, 226.
5. Hakiel, Z. TAPPI 1987, 70:113.
6. Lee, Y. M.; Wickert, J. A. J Appl Mech 2002, 69, 130.
7. Lee, Y. M.; Wickert, J. A. J Appl Mech 2002, 68, 358.
8. Tramposch, H. J Appl Mech 1965, 32, 865.
9. Tramposch, H. J Appl Mech 1967, 34, 888.
10. Qualls, W. R.; Good, J. K. J Appl Mech 1997, 64, 201.
11. Altmann, H. C. TAPPI 1968, 51:176.
12. Willett, M. S.; Poesch, W. L. J Appl Mech 1989, 55, 365.
13. Heinrich, J. C.; Connolly, D.; Bhushan, B. Tribol Trans 1984, 29, 75.
14. Lin, J. Y.; Westmann, R. A. J Appl Mech 1989, 56, 821.
15. Weick, B. L.; Bhushan, B. J Inf Stor Proc Syst 2000, 2, 1.
16. Weick, B. L.; Bhushan, B. J Appl Polym Sci 2001, 81, 1142.
17. Timoshenko, S. P.; Goodier, J. N. Theory of Elasticity; McGraw-Hill: New York, 1970.
18. Christensen, R. M. Theory of Viscoelasticity; Dover Publications, Inc.: New York, 1982.